Acoustic Backing in 3-D Integration of CMUT With Front-End Electronics

Sigrid Berg, *Student Member, IEEE*, and Arne Rønnekleiv, *Member, IEEE*

***Abstract*—Capacitive micromachined ultrasonic transducers (CMUTs) have shown promising qualities for medical imaging. However, there are still some problems to be investigated, and some challenges to overcome. Acoustic backing is necessary to prevent SAWs excited in the surface of the silicon substrate from affecting the transmit pattern from the array. In addition, echoes resulting from bulk waves in the substrate must be removed. There is growing interest in integrating electronic circuits to do some of the beamforming directly below the transducer array. This may be easier to achieve for CMUTs than for traditional piezoelectric transducers. We will present simulations showing that the thickness of the silicon substrate and thicknesses and acoustic properties of the bonding material must be considered, especially when designing high-frequency transducers. Through simulations, we compare the acoustic properties of 3-D stacks bonded with three different bonding techniques; solid-liquid interdiffusion (SLID) bonding, direct fusion bonding, and anisotropic conductive adhesives (ACA). We look at a CMUT array with a center frequency of 30 MHz and three silicon wafers underneath, having a total silicon thickness of 100 μm. We find that fusion bonding is most beneficial if we want to prevent surface waves from damaging the array response, but SLID and ACA are also promising if bonding layer thicknesses can be reduced.**

I. Introduction

Capacitive micromachined ultrasonic transducers (CMUTs) have been the subject of extensive research since the mid 1990s [1]–[3]. It has been shown that improved bandwidth may be realized by using CMUTs in medical ultrasound imaging [4]. In fabrication, photolithographic techniques developed for integrated circuit manufacturing are used. This makes high-volume production at low cost possible. It also enables the manufacturing of small elements and electrical addressing of the elements using through-wafer via interconnects for high-frequency transducer arrays for 3-D imaging [5].

One of the great benefits of using CMUT arrays as ultrasonic transducers is the relative ease of integrating the electronic circuits that are needed for transmission and reception. As a step toward integrated CMUTs and electronics, CMUT cells integrated in a standard BiCMOS process [6] and the integration of CMUT and signal-conditioning electronics on the same silicon substrate have been reported [7], [8]. With these techniques, the CMUT and electronics compete for the same die area, something that might limit both the sophistication of the electronics and the SNR. Another CMUT-on-CMOS technique is monolithic integration [9]–[11]. The CMUT is manufactured on top of an already-made CMOS circuit with analog switching electronics.

A different approach is to make electronic circuits and CMUT arrays on separate wafers and bond these to form a stack, connecting to each array element with through-wafer vias [5]. Flip-chip bonding between a 2-D CMUT array and a custom-designed integrated circuit for volumetric ultrasound imaging, using anisotropic conducting film (ACF) or using Sn/Pb solder balls has been demonstrated [12]. With flip-chip bonding techniques, several silicon wafers with electronic circuits can be bonded directly to the CMUT substrate, forming a 3-D stack. 3-D integration of electronics is advancing quickly, and new bonding techniques are being developed to bond very thin layers together. This can be beneficial in the development and design of future medical ultrasound probes.

One of the acoustic challenges in the design of CMUT transducers is the crosstalk between transducer elements resulting from acoustic coupling through the medium outside the array. Degradation in axial resolution and bright spots in the near field in imaging experiments have been observed [4]. The interaction through the fluid medium, often referred to as interface waves (Stonely-Scholte waves), has been shown both analytically [13] and experimentally [14]. Dispersive guided modes have been presented as the most important contributor to the crosstalk [15]. The present work does not consider the effects on the array responses from crosstalk at the CMUT-liquid interface.

Because of low losses and finite acoustic impedance in the silicon substrate, Lamb waves or SAWs might be generated and add to the total acoustic crosstalk in CMUT arrays. This excitation is strong when the phase velocity of the surface wave matches the phase velocity along the array of the wave excited in the fluid outside the array.

Trailing echoes in the silicon substrate are clearly observed in immersion transducers with 650 μm substrate thickness at 7 MHz [16]. The radiation patterns from unbacked CMUT transducers with 180- and 480-μm-thick substrates were compared at 4 MHz, and it was shown that Lamb waves were generated in the silicon wafer, which caused significant dips at 22° and 32° steering angles, respectively [14], [17]. It was also shown that the angle at which the dip in the radiation pattern occurs is dependent on the transmit frequency [17].

If the CMUT array is backed with a damping material, plate modes (Lamb waves) will no longer be excited

Manuscript received March 30, 2011; accepted March 1, 2012. Financial support from the Research Council of Norway through the project Smart Microsystems for Diagnostic Imaging in Medicine (project number 159559/130) is gratefully acknowledged.

The authors are with the Department of Electronics and Telecommunications, Norwegian University of Science and Technology, Trondheim, Norway (e-mail: sigrid.berg@iet.ntnu.no).

DOI http://dx.doi.org/10.1109/TUFFC.2012.2353

0885–3010/$25.00 © 2012 IEEE

because of the losses and the thickness of the structure. However, SAWs might still be generated. Although the forces on the top electrode serve to launch acoustic waves into the medium of interest, equal forces are placed on the membrane support and substrate electrode. If undamped waves exist in the substrate, they can be excited by these forces and significantly reduce the efficiency of the transducer at frequencies near possible substrate resonances. At certain steering angles, the surface displacement from the SAW will be almost in phase with the membrane vibrations, and the excited wave will be enhanced. At a slightly different steering angle, the two displacements are out of phase, and the excitation goes through a minimum. The SAW is exponentially damped as it penetrates into the substrate, so for the acoustically absorbing backing to damp the surface wave, the substrate cannot be too thick. If the thickness exceeds a certain limit, the acoustic impedance of the surface may become close to or lower than the acoustic impedance of the fluid (1.5 MRayl for pure water). In such cases, the resonance and antiresonance might severely affect the transmit efficiency. Such resonances were observed in the CMUT model presented in [18].

This paper attempts to address the problems caused by acoustic ringing in stacks of 2-D CMUT arrays on top of three integrated circuit (IC) wafers and an absorbing backing, as illustrated in Fig. 1. The materials introduced by the bonding generally have lower acoustic velocities than silicon, hence the penetration depth of the SAW is reduced when several silicon layers are bonded together. The backing material must therefore be closer to the top surface to absorb the SAW.

Our model mainly considers a well-backed array extending infinitely in the x and y directions. In some special cases, it will also be considered how a finite array will be affected by the SAW. We will also show that Lamb waves may degrade the response if the substrate wafer is left unbacked. Simulations of an unbacked CMUT structure are compared with measurements from Jin *et al.* [14], [17]. The possibility of including an intermediate damping layer between the CMUT array and the first circuit layer to damp some of the acoustic energy before it penetrates further into the stack will also be investigated. This work is based on the work presented in [18]–[20].

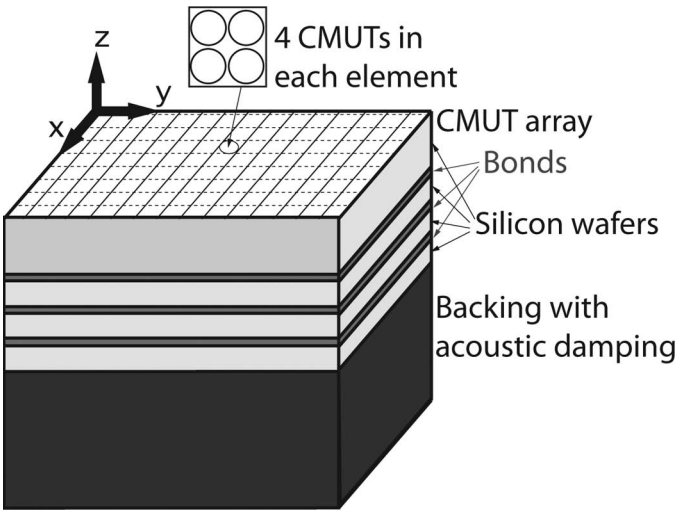

Fig. 1. Illustration showing a part of the infinite CMUT array mounted on silicon wafers for electronics and a backing structure.

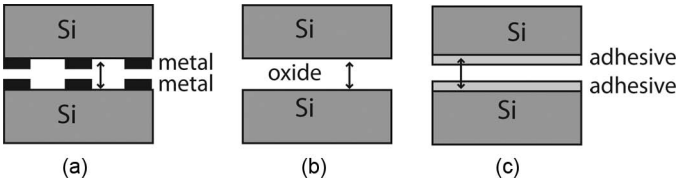

Fig. 2. Illustration of the three bonding techniques investigated in this work: (a) metal-to-metal bonding [e.g., solid-liquid interdiffusion (SLID)], (b) direct fusion bonding, and (c) adhesive bonding.

II. Bonding Techniques

Three different bonding techniques are analyzed in this work, solid-liquid interdiffusion (SLID) bonding, direct fusion bonding, and anisotropic conductive adhesives (ACAs), all illustrated in Fig. 2.

Solid-liquid interdiffusion bonding (SLID) is a promising bonding technique for 3-D circuit integration. The bonding process results in a three-layer metal stack as a bonding layer. It consists of copper at the top and bottom and a copper-tin alloy (Cu_3Sn), in the middle [21]–[23]. Some gaps are needed in the SLID bonding layer to avoid connecting adjacent elements electrically, but if the distance between contact pads is large, most of the area between the pads can be covered with a dummy SLID layer, to minimize the air gaps and increase the area with mechanical contact.

In direct fusion bonding, two extremely smooth wafer surfaces are brought into very close contact so that intermolecular Van der Waals attractive forces and surface OH bonds create a weak bond between the wafers. This might be done at room temperature. With further annealing at higher temperatures covalent bonds are formed. Most commonly, SiO_2–SiO_2 surfaces are used [24]. This bonding technique results in a thin layer of SiO_2 between the silicon wafers and connection between metal pads on the respective circuit wafers [25].

ACAs consist of a very stable adhesive polymer matrix containing 2- to 7-μm diameter metal or metal-coated spheres. The cured adhesive provides mechanical attachment and immobilizes the deformed conductive particles. Because of the deformation of the conducting particles, the stand-off height between the pads is around 50% of the starting diameter of the particles [26]. It has been demonstrated that anisotropic conductive film (ACF) can be used as an interconnect technology for micro electromechanical systems (MEMS) devices [27].

III. CMUT Model

The simulations in this work are based on an analytical CMUT model [19].[1] In addition to the desired radiation into the fluid, the motion of the CMUTs may also couple to waves in the support structure. It is well known that this may degrade the array performance [14]. Equations to analyze this degradation are developed here. The model describes the motion of the membrane as a combination of N free acoustic modes of an acoustically isolated CMUT, and how these modes are coupled to the applied voltages and the fluid outside the CMUTs. In the present work, we also include the acoustic coupling to the support structure, which in this case is a stack of silicon wafers with acoustic backing material at the bottom.

The total vibration amplitude of a point on the array surface is hence given by

$$W_{\text{tot}}(\vec{r},\vec{k}_{\|}) = W_0 e^{-j\vec{k}_{\|}\vec{r}} + \sum_{n=1}^{N} W_n w_n(\vec{r}-\vec{r}_n), \qquad (1)$$

where $\vec{k}_{\|}$ is the k-vector component along the surface of the array of the wave excited in the fluid. The movement of the CMUT membrane surface relative to the nominal substrate surface is expressed as a sum over the acoustic eigenmodes of the CMUT, with amplitude profiles $w_n(\vec{r}-\vec{r}_n)$ where $\vec{r}_n$ is a reference point (center) of each mode and the $\vec{r}$ gives a position on the array surface. The w_n values are normalized to a peak value of 1 and, hence, the constants W_n give the peak deflection in mode n. The vertical sinusoidal deflection amplitude of the nominal substrate surface is denoted by W_0. For a thin membrane, the set of modes which are included here have membrane velocities essentially in the $+z$-direction of Fig. 1. Modes with velocities in the transverse direction do not radiate into the fluid, and are normally not excited. In addition, the membranes also have a dc deflection W_{DC}.

The eigenmodes are chosen to be the modes of the free circular CMUT membrane with fixed support, unaffected by external acoustic or electric pressures. In this situation the modes are orthogonal with the following scalar product:

$$\int_A m w_m w_n \mathrm{d}A = \delta_{m,n} M_n. \qquad (2)$$

Here, A is the membrane area, and m is the mass per unit area of the membrane. This may vary over the membrane. $\delta_{m,n}$ is the Kronecker delta equal to 1 when $n=m$, otherwise zero. M_n becomes the effective mass of mode n.

The wave excited in the substrate will give a slight curvature to the array surface and modify the mode properties. We neglect those effects in these simulations. As long as the substrate motion is low, the approximation is believed to be valid. However, if the substrate vibration amplitude, W_0, is large, and there are few CMUTs per wavelength, the bending of the substrate across one CMUT should be accounted for. We have not looked at this, because such an array will not work well for imaging for other reasons.

It is interesting to note that a force with the shape mw_n over the membrane will accelerate the membrane mass to give a velocity distribution over the membrane exactly described by w_n times a constant. It follows that for excitation of the membrane modes, the effective forces $F_n^{(\text{eff})}$ are equivalent to a distributed force F_z in the z-direction over the membrane, where

$$F_n^{(\text{eff})} = \int_A F_z w_n \mathrm{d}A. \qquad (3)$$

Each of these forces accelerates only one mode, mode n, with an equivalent mass M_n given by (2) and an equivalent spring constant

$$F_n^{(\text{s})} = \omega_n^2 M_n, \qquad (4)$$

where ω_n is the resonance frequency of mode n.

There are several external forces that are acting on the membrane, and which determine the amplitudes W_n through (11). Most of these are discussed in detail in [19] and appropriate formulas are given here. They are given for a biased CMUT with an added small signal voltage. First, there is the added electrostatic force resulting from the small signal voltage v, giving the force $K_n^{(\text{v})}v$ on mode n. In addition there is the electrostatic forces resulting from a small signal deflection $W_m w_m$, giving the forces $K_{n,m}^{(\text{w})}W_m$ on mode n. Further, the reaction force from the fluid on mode n as a result of the motion in mode m, $j\omega Z_{n,m}^{(\text{me})}W_m$ is added.

The pressure in the fluid leads to normal forces acting on the array surface. We assume that the small signal velocity $i\omega W_m w_m$ leads to a normal tension on the array surface $t_{zz,m}^{(\text{me})}(x,y)$, which results in a normalized driving force for the nth mode given by the acoustic impedance and the velocity, $i\omega W_m Z_{n,m}^{(\text{me})}$. This leads to an expression for the acoustic impedance:

$$Z_{n,m}^{(\text{me})} = \frac{1}{j\omega W_m}\int_A t_{zz,m}^{(\text{me})} w_n \mathrm{d}A, \qquad (5)$$

which is the main part of the fourth matrix in (11). This impedance takes the variation of tension and mode velocity over the membrane into account. From this, it follows that the deflection in one mode causes forces from the fluid driving the same and other modes. The deflection $W_0 e^{-j\vec{k}_{\|}\vec{r}}$ of the top surface gives the pressure $t_{zz,0}^{(\text{me})}$ on the top surface, also containing the exponential variation. The

[1] There are some errata in [19]: The right side of the equation for $P'(k_{x'})$ in [19, Eq. (23)] should be divided by ω, and the pressure P_l in [19, Eq. (24)] is for a unit deflection in mode l. In addition, P_{cr} on the right side of [19, Eq. (26)] should be P_{el}.

$$-\omega^2\begin{bmatrix} M_{00} & M_{01} & \cdots & M_{0N} \\ M_{10} & M_1 & 0 & 0 \\ \vdots & 0 & \ddots & 0 \\ M_{N0} & 0 & 0 & M_N \end{bmatrix}\begin{bmatrix} W_0 \\ W_1 \\ \vdots \\ W_N \end{bmatrix} + \begin{bmatrix} j\omega Z_{\text{surf}} & 0 & \cdots & 0 \\ 0 & F_1^{(\text{s})} & 0 & 0 \\ \vdots & 0 & \ddots & 0 \\ 0 & 0 & 0 & F_N^{(\text{s})} \end{bmatrix}\begin{bmatrix} W_0 \\ W_1 \\ \vdots \\ W_N \end{bmatrix} - \begin{bmatrix} 0 & 0 & \cdots & 0 \\ 0 & K_{1,1}^{(\text{w})} & \cdots & K_{1,N}^{(\text{w})} \\ \vdots & \vdots & \ddots & \vdots \\ 0 & K_{N,1}^{(\text{w})} & \cdots & K_{N,N}^{(\text{w})} \end{bmatrix}\begin{bmatrix} W_0 \\ W_1 \\ \vdots \\ W_N \end{bmatrix}$$
$$+ j\omega\begin{bmatrix} Z_{00} & Z_{01} & \cdots & Z_{0N} \\ Z_{10} & Z_{1,1}^{(\text{me})} & \cdots & Z_{1,N}^{(\text{me})} \\ \vdots & \vdots & \ddots & \vdots \\ Z_{N0} & Z_{N,1}^{(\text{me})} & \cdots & Z_{N,N}^{(\text{me})} \end{bmatrix}\begin{bmatrix} W_0 \\ W_1 \\ \vdots \\ W_N \end{bmatrix} = \begin{bmatrix} 0 \\ K_1^{(\text{v})} \\ \vdots \\ K_N^{(\text{v})}. \end{bmatrix} v \tag{11}$$

corresponding effective forces on the membrane modes are denoted $j\omega W_0 Z_{n0}$ for $n \geq 1$, where

$$Z_{n0} = \frac{1}{j\omega W_0}\int_A t_{zz,0}^{(\text{me})} w_n \mathrm{d}A. \tag{6}$$

Because the membranes with their mode profiles w_n, $n \geq 1$, are riding on the movement of the substrate, the membrane mode n sees acceleration forces due to the deflection $W_0 e^{-j\vec{k}_\parallel \vec{r}_n}$, which we write $-\omega^2 M_{n0} W_0$, where

$$M_{n0} = \int_A m w_n e^{-j\vec{k}_\parallel \vec{r}} \mathrm{d}A. \tag{7}$$

The amplitude of the substrate movement W_0 is determined by the forces acting on the surface and the acoustic impedance Z_{surf}, which relates the amplitude W_0 to the $\vec{k}_\parallel$ Fourier component of the forces on the surface. Hence, the contribution to this Fourier component from real space forces are found through a Fourier transform. The calculation of Z_{surf} is discussed later. The forces influencing W_0 include the reaction forces from accelerating the membrane uniformly to give W_0, and the reaction forces from accelerating all different modes, which we write as $-\omega^2 M_{00} W_0$ and $-\omega^2 M_{0n} W_n$, respectively. All forces are per unit area. Hence, we have

$$M_{00} = \frac{1}{A_\text{e}}\int_{A_\text{e}} m \mathrm{d}A, \tag{8}$$

$$M_{0n} = \frac{1}{A_\text{e}}\int_A m w_n e^{j\vec{k}_\parallel \vec{r}} \mathrm{d}A, \tag{9}$$

where A_e is the area of an element.

Finally, the $\vec{k}_\parallel$-component of the forces on the surface from the fluid resulting from movement of mode n, $n \geq 0$, $j\omega Z_{0n} W_n$, also must be added. The acoustic impedance Z_{0n} is given by

$$Z_{0n} = \frac{1}{j\omega W_n A_\text{e}}\int_{A_\text{e}} t_{zz,n}^{(\text{me})} e^{j\vec{k}_\parallel \vec{r}} \mathrm{d}A. \tag{10}$$

Note that these impedances are per-area acoustic impedances.

The result is a matrix equation system, from which we solve the excitation amplitudes W_n of the acoustic eigenmodes of the membrane and the substrate vibration amplitude W_0, for a small signal voltage, v. Eq. (11), see above, is an expanded version of [19, Eq. (10)].

More details on certain parts of (11) are given in the following paragraphs. An important parameter in the derivation of the equivalent electrostatic forces is the capacitance C_m of the CMUT. We use the approximation of a parallel plate capacitor and disregard fast transversal changes in the distance between capacitor plates and the build-up of charge on the edges of the capacitor plates, and get

$$C_m = \int_{\text{electrode}} \frac{\varepsilon_0 \mathrm{d}A}{\Sigma h_i/\varepsilon_r^{(i)} - W_{\text{DC}}}, \tag{12}$$

where ε_0 is the dielectric constant in vacuum and $\varepsilon_r^{(i)}$ and h_i are the relative dielectric constant and thickness of the dielectric material between the electrodes. In our model, $i = 1{,}2$, where h_1 corresponds to the thickness of silicon nitride membrane and h_2 is the height of the vacuum gap. Correction terms due to additional capacitances and forces on the edges of the electrodes could be included. Equivalent electrostatic forces for mode n, acting on the membrane as a result of the small signal voltage, v, and a small signal deflection $W_m w_m$ in mode m, where m might be different from n, are $K_n^{(\text{v})} v$ and $K_{n,m}^{(\text{w})} W_m$ respectively, where $K_n^{(\text{v})}$ and $K_{n,m}^{(\text{w})}$ are given by

$$K_n^{(\text{v})} = \int_{\text{electrode}} \frac{\varepsilon_0 V_0 w_n \mathrm{d}A}{(\Sigma h_i/\varepsilon_r^{(i)} - W_{\text{DC}})^2} \tag{13}$$

$$K_{n,m}^{(\text{w})} = \int_{\text{electrode}} \frac{\varepsilon_0 V_0^2 w_n w_m \mathrm{d}A}{(\Sigma h_i/\varepsilon_r^{(i)} - W_{\text{DC}})^3}. \tag{14}$$

Both integrals are taken over the area where the capacitor electrodes are overlapping, and are based on the assumption that the small signal per-area forces on the membrane resulting from small signal voltage v and deflection w, are given by $V_0 c_{m'} v$ and $V_0^2 c_{m''} w$, respectively [2]. $c_{m'}$ and $c_{m''}$ are the first and second derivatives of the per-area capacitance, c_m, with respect to the distance between electrodes.

To account for the acoustic properties of the backing material, the circuit wafers, and the bonding layers, the acoustic impedance of the substrate surface, Z_{surf}, for a given frequency ω and k-vector along the surface, $\vec{k}_{\parallel}$, can be calculated using a matrix method described by Adler [28]. We describe the acoustic waves at the bottom of the silicon substrate (or stack of silicon layers) as a combination of one longitudinal and two shear waves, all with the k-vector component $\vec{k}_{\parallel}$ in the xy-plane shown in Fig. 1. At the bottom of the structure, there may exist three linearly independent wave fields of longitudinal and shear waves given as

$$\tau_{\text{bottom}} = \begin{bmatrix} T_{xz}^{l} & T_{xz}^{s1} & T_{xz}^{s2} \\ T_{yz}^{l} & T_{yz}^{s1} & T_{yz}^{s2} \\ T_{zz}^{l} & T_{zz}^{s1} & T_{zz}^{s2} \\ v_{x}^{l} & v_{x}^{s1} & v_{x}^{s2} \\ v_{y}^{l} & v_{y}^{s1} & v_{y}^{s2} \\ v_{z}^{l} & v_{z}^{s1} & v_{z}^{s2} \end{bmatrix} \begin{bmatrix} A \\ B \\ C \end{bmatrix}, \tag{15}$$

where T_{xz}, T_{yz}, and T_{zz} give stresses; v_x, v_y, and v_z give the particle velocities; and A, B, and C are unknown wave amplitudes. The wave fields should be chosen in accordance with the boundary conditions at the bottom of the structure. If the stack ends in a volume that does not give any reflected waves, its lower layer could be considered semi-infinite, and at the top of that layer only one longitudinal and two shear waves propagating or decaying into that layer could exist. Because the normal stresses and particle velocities are continuous over a boundary, the wave fields of the bottom layer are directly represented in (15). If the bottom layer ends in a surface which may give reflections back to the stack, we must know the reflection coefficient of the waves at the bottom surface. The fields of (15) are then a linear combination in accordance with the reflection coefficients of the three waves propagating or decaying upwards and the three waves propagating or decaying downwards in the bottom layer.

The total transformation of velocities and stresses from the bottom of the stack to the top through layers from 1 to K is as follows:

$$\tau_{\text{surface}} = \Phi \tau_{\text{bottom}}, \tag{16}$$

where

$$\Phi = \prod_{k=1}^{K} \phi_k(h_k, M_k). \tag{17}$$

The thickness of layer k is denoted h_k, and ϕ_k is, in this case, a 6×6 matrix which is a function of material constants M_k, the frequency ω, and $\vec{k}_{\parallel}$ of the excitation at the array surface.

We assume that there are no shear stresses at the top surface of the stack ($T_{xz,\text{surface}} = 0$ and $T_{yz,\text{surface}} = 0$). This gives two relations between the three constants in (15), and we can find the acoustic impedance at the substrate surface as

$$Z_{\text{surf}} = \frac{T_{zz,\text{surface}}}{v_{z,\text{surface}}}, \tag{18}$$

and, hence, (11) can be solved. For details about the mathematics of the method, we refer to Adler [28].

IV. Results

To validate the model, we present simulations (Matlab 7.8, The MathWorks, Natick, MA) of a CMUT structure without backing vibrating in vegetable oil, and compare the simulation results with measurements presented in literature. Both the front and the back side of the structure are loaded by the oil. Further, we use the model (with backing) to investigate the acoustic properties of the stacks described in Section IV-B, and look at how thinner bonding layers and lower reflection loss at the array bottom affect the response of an infinite array. In addition, we investigate how the response from a finite array is affected by the surface acoustic wave in the silicon substrate.

A. Model Validation

Jin *et al.* have shown the radiation patterns from a single CMUT element consisting of 8×160 circular CMUTs, each with a radius of 15 μm, as a function of steering angle [17]. The CMUTs have a center frequency of around 4 MHz. To validate the CMUT model used in this work, we have simulated a similar CMUT element, radiating into olive oil, and sampled the signal at a distance of 9.4 cm from the transducer. The main feature in the measurements that should be captured by the modeling is the interference resulting from plate modes excited in the silicon wafer and radiated into the fluid, to a large degree outside the CMUT elements. Considering this, some adjustments of the model must be made. Our model is based on infinite arrays covered with CMUTs, where we may excite only a limited area, in this case, an 8-CMUT-wide strip. The simulated array has no acoustic backing, hence the back surface acts like a free surface. In such a configuration, plate modes (Lamb waves) will be excited in the silicon wafer as a result of the vibrations of the membranes. To couple efficiently to the fluid, CMUTs must have an acoustic impedance similar to that of the fluid outside, 1.35 MRayl for olive oil, and much lower than silicon, 19.6 MRayl. Hence, normal CMUTs on the unexcited parts of the array in our model will act as cushions, preventing the movement in the silicon to be transferred to the fluid. Because our interest is mainly to compare the radiation into the fluid directly from the CMUTs with the radiation due to the plate modes, we may increase the stiffness of the CMUTs, to reduce the cushioning. As this stiffness becomes very large, the cushioning action of the

non-active CMUTs in our model disappears, and the relation between waves in the fluid that are directly excited by the CMUTs and those excited by the plate modes will be as in the experiment. The efficiency of the CMUTs will, however, be poor.

In Fig. 3, we see that the angle at which the response has a dip depends on the frequency, and that the simulations and the measurements match well. Both the A0 mode and the S0 mode of the Lamb waves are evident. The A0 mode occurs between 20° and 25°, whereas the S0 mode is excited at about 12° to 14°. The angles at which the dips in the radiation occur depend on several factors, such as wafer thickness, the distance between the transmitter and the receiver, the size of the wafer, and the conditions at the edge of the wafer/chip. However, there is limited information in [17] about the size of the silicon wafer on which the single CMUT element is fabricated and how the wafer or chip is mounted in the measurement setup. We have assumed a chip size of 0.87 cm and that the plate modes are damped at the edge of the chip.

When comparing the radiation from an array on 180- and 480-μm-thick silicon wafers, we see from Fig. 4 that the dip is moved from 22° to 32°, both in the simulations and the measurements from Jin *et al.* [14], [17]. The measured response of the 180-μm wafer drops off rapidly above 33°, both compared with our simulation and to the measurements on the 480-μm wafer. This must be the result of unknown factors in the experiment.

B. Array Configurations With Acoustic Backing

In invasive applications such as intravascular imaging, CMUT technology could be of great advantage because of the possibility of miniaturization and integration of electronic circuits. To reduce the cable count from the transducer, signal processing, such as amplification and a major part of the beamforming, should preferably be done at the transducer end of the cable. To achieve this, we must stack integrated electronic circuits underneath the array. Depending on the application of the transducer, the need for front-end processing and the number of circuit layers may vary. One might need separate layers for high-voltage transmit electronics, low-voltage receive electronics, beamforming, and communication.

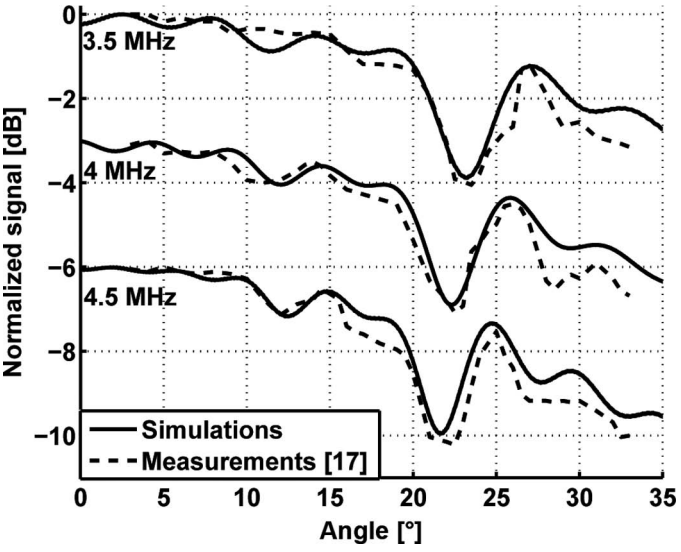

Fig. 3. Comparison of measurements presented by Jin *et al.* [17] and the response from the CMUT model. In the model, there is no backing material behind the silicon wafer, so the bottom of the silicon wafer is modeled as a free surface vibrating in vegetable oil. The data at 3.5 MHz are normalized with 0 dB as the maximum, whereas the data at 4 and 4.5 MHz are shifted to −3 and −6 dB, respectively.

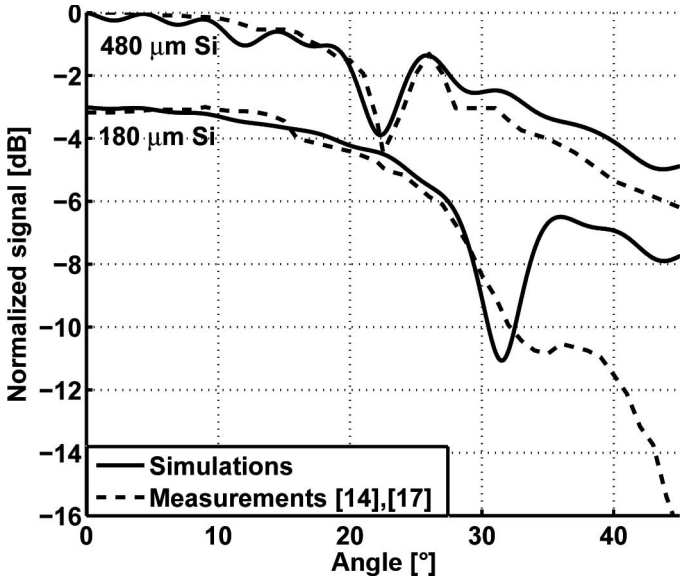

Fig. 4. Comparison of measurements presented by Jin *et al.* [14], [17] and the response from the CMUT model. The responses from arrays with different substrate thicknesses are compared. The data from the 480-μm-thick wafer are normalized with 0 dB as the maximum, whereas the maximum of the data from the 180-μm wafer is shifted to −3 dB.

To show the feasibility of such a probe, we have simulated the response from stacks with a CMUT array on top of three integrated circuit wafers that are bonded with the three different bonding techniques described previously, and backed with a tungsten-epoxy composite. All of the silicon wafers are assumed to be of 100 orientation.

We take as an example an array of circular CMUTs arranged in a regular square grid. In principle, the wave from such an array can be steered in all directions. To illustrate the beam steering, we choose to only steer along one of the main axes. In such a configuration, each transducer element consists of two infinite lines of CMUTs, resulting in an element width of 25 μm. At a center frequency of 30 MHz, the element width corresponds to half a wavelength in water. The coupling coefficient, k^2, is calculated based on the fixed and free capacitances of the transducer [29]. Table I shows the geometric and electric properties of the CMUTs.

To simulate the acoustic properties of the three different bonding techniques, we include five different wafer stacks in the simulations. The first is a pure silicon wafer; in the second and third stacks, all of the silicon interfaces are bonded with fusion bonding and SLID, respectively. The two last stacks have been named 4a and 4b, and both

TABLE I. PROPERTIES OF CMUT ARRAY USED IN SIMULATIONS.

CMUT radius	5.7 μm
CMUT pitch (center to center)	12.5 μm
Cavity depth	60 nm
Total membrane thickness	470 nm
Membrane, mass per area	1.4 g/m^2
Membrane, bending stiffness per unit width	2.26 GN·m
Collapse voltage	63.75 V
DC bias voltage	61.75 V
Coupling coefficient, k^2	0.50
Center frequency	30 MHz
Bandwidth	130%

use anisotropic adhesive (ACA) as the bonding material. In Stack 4b, we introduce an intermediate damping layer between the first ACA layer and the first circuit wafer to absorb some acoustic energy before it penetrates into the circuit layers. All of the stacks are backed with 200-μm tungsten-epoxy. Table II lists the geometric details and Table III lists the elastic properties of the materials in the stacks included in the simulations. Fig. 5 illustrates their composition.

Both damping layers in the simulations are composites made of epoxy (EPO-TEK 353 ND from Epoxy Tech. Inc., Billerica, MA) and tungsten and have properties that are calculated according to [35]. Details are given in Table IV. The table also gives the loss at 30 MHz for both damping materials. Both composites are assumed to have a mechanical Q of 16. It is assumed that the bottom backing layer may be cast directly on the layers above, with no need for a separate bonding layer. The intermediate damping layer will need vias for electrical signals to and from all the CMUT elements in the array. The acoustic effect of the vias is not taken into account in these simulations. The layer cannot be conducting, so the tungsten fraction is set to 35%. We expect to need separate bonding layers on both sides of the composite.

We assume that the CMUT operates in rapeseed oil in these simulations. It has a shear viscosity of 72 mPa·s at 20°C, a density of 910 kg/m^3, and speed of sound of 1425 m/s. The rapeseed oil is chosen because of its high viscosity, to suppress the effect of cross-coupling through the fluid.

In addition to the stacks in Table II, we have investigated how future improvements in the bonding techniques leading to thinner bonding layers may result in less ripple in the array response.

C. Infinite Array Responses

1) Frequency Response: The frequency responses presented here are from simulations of an infinite array which is transmitting into a fluid medium. The results presented are also valid for reception because of reciprocity.

In Fig. 6, we show the transmitted power as a function of frequency and steering angle from CMUT arrays on pure silicon substrates of thickness 50 and 100 μm, which are well backed by a tungsten-epoxy composite. We see that the strength of the unwanted resonance depends strongly on the thickness of the substrate, but unlike Figs. 3 and 4, we see that the angle of the response dip does not change as a function of frequency in this case. This is because the dip here is caused by a mainly non-dispersive SAW rather than dispersive plate modes. Increasing the substrate thickness from 50 and 100 μm leads to increased ripple, and results in a dip of −1.5 dB at the center frequency, 30 MHz. The effect is even stronger at higher frequencies. At 45 MHz, which is the upper frequency of 100% bandwidth, the dip of the transmitted power from the array with a 100-μm-thick substrate is −16 dB. The ripple around 20 MHz in Fig. 6 is due to element-to-element crosstalk in the CMUT-fluid interface. This crosstalk would be much more severe if the transducer had radiated into a low viscosity fluid such as pure water.

These results apply to infinite arrays, for which we see that the dip in the amplitude response is very deep. However, it is narrow in steering angle, and the effect will not be as severe in finite arrays, especially if the arrays are small in area. This is the case as the SAW grows slowly along the array.

In Fig. 7, we show the response at 30 and 45 MHz versus steering angle for the first four stacks described

TABLE II. CMUT AND ELECTRONICS STACKS USED IN SIMULATIONS.

	Bonding method	CMUT wafer thickness, μm	Circuit wafer thickness, μm	Bond thickness, μm
1	Pure silicon	100	NA	NA
2	Fusion bond	25	3 × 25	2
3	SLID bond	25	3 × 25	8
4a	ACA/	25	3 × 25	2
4b	ACA/interm. damping	25	3 × 25	2/100

TABLE III. ELASTIC PROPERTIES OF MATERIALS IN THE 3-D STACKS.

Material	ρ [kg/m^3]	c_{11} [GPa]	c_{12} [GPa]	c_{66} [GPa]
Silicon (100) [30]	2332	165.7	63.99	79.56
SiO_2 [31]	2203	78.85	16.1	Isotropic
Cu [32]	8600	215.8	127.2	Isotropic
Cu_3Sn [33]	8900	c_{11}: 154.6 c_{22}: 173.7 c_{33}: 148.2	c_{12}, c_{21}: 78.9 c_{13}, c_{31}: 76.5 c_{23}, c_{32}: 95.1	c_{44}: 50.2 c_{55}: 44.2 c_{66}: 55.0
EPO-TEK 353 [34]	1240	9.51	5.76	Isotropic

in Table II. The ripple at 30 MHz is −1.5 dB in Stack 1, which is pure silicon. When bonding layers are added to the stack without changing the total amount of silicon, the dip increases. Fusion bonding in Stack 2 shows a −2 dB dip, whereas SLID bonding in Stack 3 and ACA in Stack 4a give −7.5 and −6 dB dips, respectively. The interaction with the surface acoustic wave becomes stronger at higher frequencies. At 45 MHz, the dip in transmitted power is between −16 and −23 dB, depending on the composition of the stack. The added ripple compared with Stack 1 is caused by the added bonding materials, caused by poor impedance match between silicon and the various bonding materials, and by added total thicknesses.

Depending on the composition of the stack, the angle at which the SAW couples to waves in the fluid varies. It is the relationship between the velocity of the surface acoustic wave in the stack and the velocity of sound in the fluid that decides the steering angle at which the energy couples to the SAW. Stacks with low wave velocity compared with silicon result in higher coupling angles, such as Stacks 3 and 4, whereas in Stacks 1 and 2, the coupling occurs at lower angles. To bring the SAW coupling outside a steering angle range of ±45°, which is commonly used in imaging, the effective SAW velocity must be lower than 1500 m/s $\times \sqrt{2} \approx$ 2100 m/s when the imaging medium is water.

To show the effect of improved bonding techniques, we present simulations in which the thicknesses of the bonding layers are reduced by a factor of three in Stacks 3 and 4a. This leads to a reduction of the ripple by 65% and 55% at 30 MHz in Stacks 3 and 4a, respectively, as seen in Fig. 8.

We see from the left plot in Fig. 8 that the peak and dip of the response curve changes from 25.5° to 21.5° as the SLID layer thickness is reduced. This is due to the increased effective SAW velocity in the stack caused by the reduced metal thicknesses.

We have calculated the error signal caused by the SAW in an infinite array. The error is defined as the difference between the transmitted pressure which is affected by the coupling to the SAW and an ideal transmitted pressure, which is a best smooth approximation to the calculated response. The energy of the error signal is found by integrating the squared error in the pressure over a certain span in frequency and angle, and it is compared with the energy of the smooth response over the same range. We have chosen to present the energy of the error signal from 15 to 45 MHz over a sector of 10°, where the coupling to the surface acoustic wave is strong. This is shown in Fig. 9 for Stacks 1, 2, 3, and 4a. We see how the various bonding materials affect the total error, and it is shown that the energy of the error signal varies by more than 15 dB from a pure silicon wafer of 50 μm to a stack of 4 × 12.5 μm silicon wafers bonded with three layers of SLID.

For the stacks in which four silicon layers are bonded together, we assume that all the Si layers have the same thickness. Hence, each layer is one fourth of the total given thickness.

2) Intermediate Damping Layer: Using SLID and ACA results in bonding layers which damp the surface acoustic waves poorly. In these cases, we propose an intermediate damping layer between the CMUT array and the first circuit wafer to damp some of the acoustic energy before it penetrates further into the stack. In the left plot of Fig. 10, we see the transmitted power from Stack 4a versus frequency and steering angle, where there is ACA between all silicon layers. The response has a severe resonance at 25° because of the lack of damping of the SAW. We introduce an intermediate damping layer of 100 μm, using tungsten-epoxy composite with only 35% tungsten to keep it non-conducting. From the right plot in Fig. 10, we see that the unwanted resonance at 25° is reduced, but there is still some ripple left at high frequencies, and some new ripple is introduced in the low-frequency range. This might lead to high-amplitude ringing in the impulse response. A better acoustic match between the damping layer and silicon, using close to 45% tungsten, would reduce the ringing.

TABLE IV. MATERIAL PROPERTIES OF DAMPING LAYERS [35].

	ρ [kg/m^3]	v_l [m/s]	v_s [m/s]	Z_a [MRayl]	Loss [dB/mm]	W [% vol]
Bottom backing	9676	2024	1097	19.6	24.7	47.5
Intermediate	7465	1724	886	12.9	29.0	35

D. Excitation of a Finite Array

The model describes the response from an infinite array. Because, in all practical applications, an ultrasound array will be of finite size, we include simulations in which only a finite part of an infinite array is excited. It is especially interesting to see how the response from an array is affected by the surface acoustic wave in the substrate, and we show both how plane waves and focused beams are affected by the coupling to the SAW.

In the model, the area surrounding the excited CMUTs is in principle also covered with CMUTs that can vibrate as a result of the excitation of their neighbors. However, in the simulations of a finite array we have set the velocity in the z-direction of the surface to zero outside the excited part of the array.

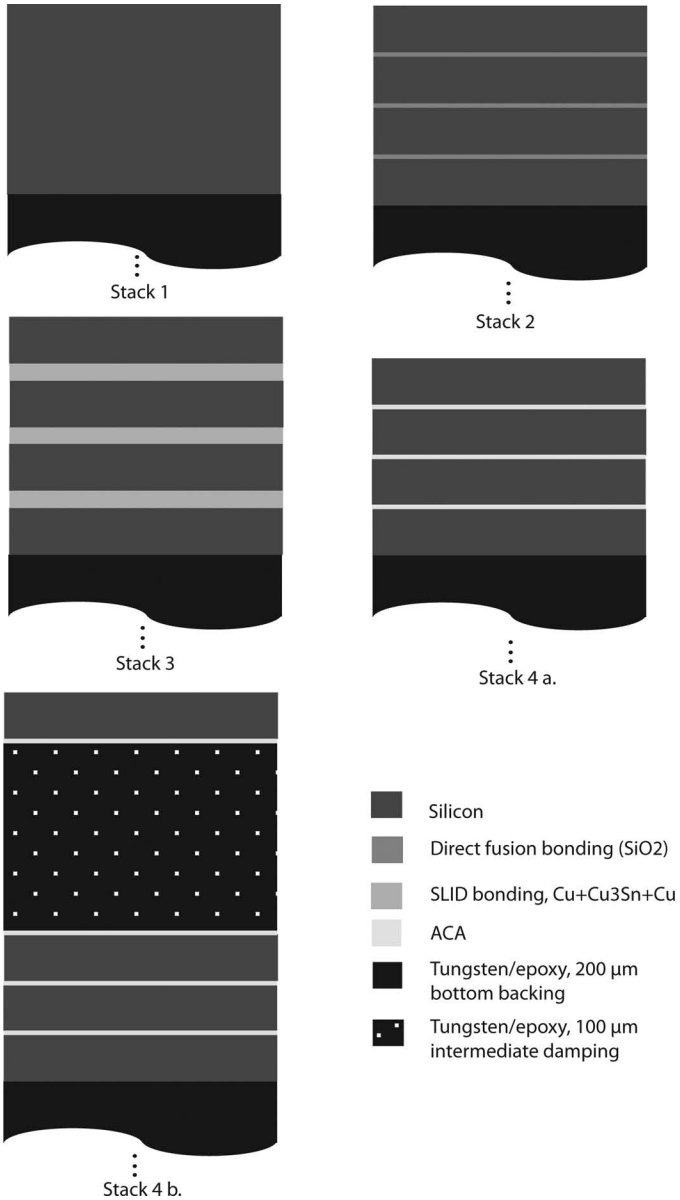

Fig. 5. Illustration of the five stacks we have included in the simulations. All the stacks are backed with 200 μm of tungsten-epoxy composite described in Table IV.

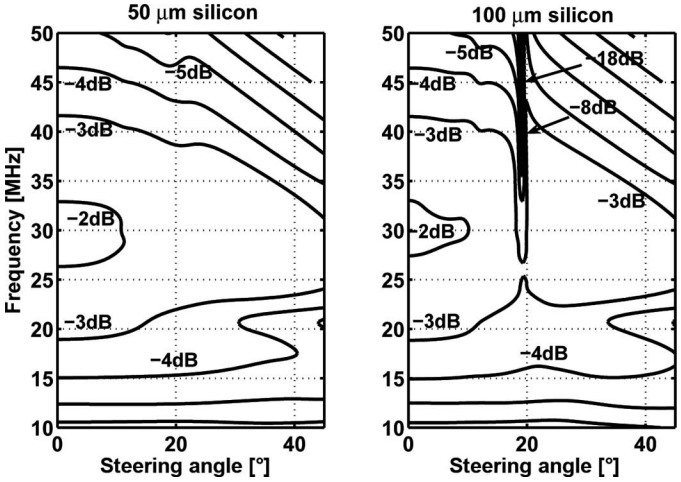

Fig. 6. The transmitted power into rapeseed oil from the CMUT array on silicon substrates of (left) 50 μm and (right) 100 μm as a function of steering angle and frequency. There is 1 dB between the lines. The substrate is backed by a 200-μm tungsten-epoxy composite with 47.5% volume fraction of tungsten, as described in Table IV.

The simulation results shown in Figs. 6 to 10 are all from an infinite CMUT array model. In Figs. 11 to 13, we show how the response from an array of finite size is affected by the substrate ringing. The surface acoustic wave will be generated when the CMUT membranes vibrate, and its amplitude will increase along the array. Hence, the effect will be minimal for very small arrays, whereas in larger arrays, the SAW might cause image artifacts. In Fig. 11, we show how the amplitude of the radiated pressure decreases along the array, when a plane wave is steered +17.75° off broadside for a 3.2-mm-wide array at 30, 37.5, and 45 MHz. The peaks at the 1.6-mm end of the arrays comes because the excitation here is due to excitation of a broad range of k-vectors, and the net result is not completely out of phase with the excitation through the SAW.

The array consists of 128 elements, with two lines of CMUTs of width 12.5 μm, in each element. It is shown that the effect of the SAW increases with frequency, and

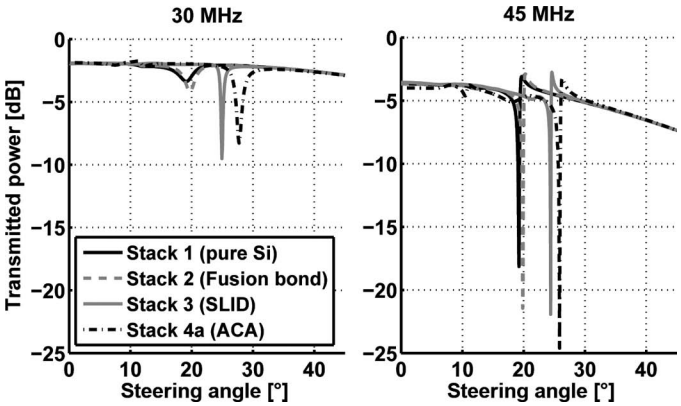

Fig. 7. The transmitted power at 30 and 45 MHz versus steering angle into rapeseed oil from the stacks with a CMUT array on top of three circuit wafers. The stacks are described in Table II.

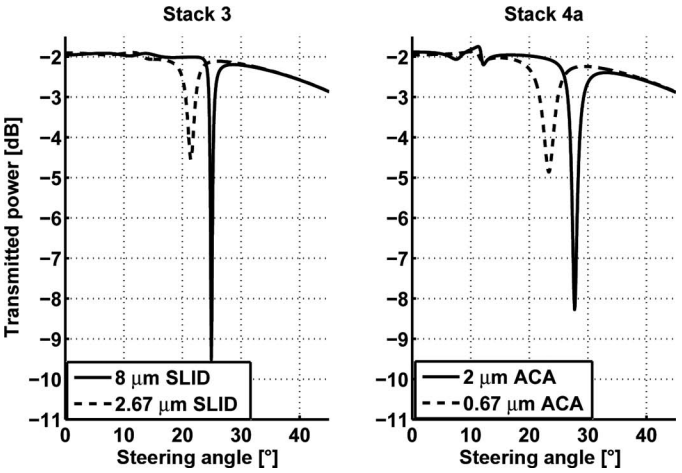

Fig. 8. The transmitted power at 30 MHz from stacks with (left) solid-liquid interdiffusion (SLID) bonding and (right) anisotropic conductive adhesives (ACA). The solid line represents the original configuration, whereas the dotted lines show the stacks with bonding layer thicknesses which are reduced by a factor of three.

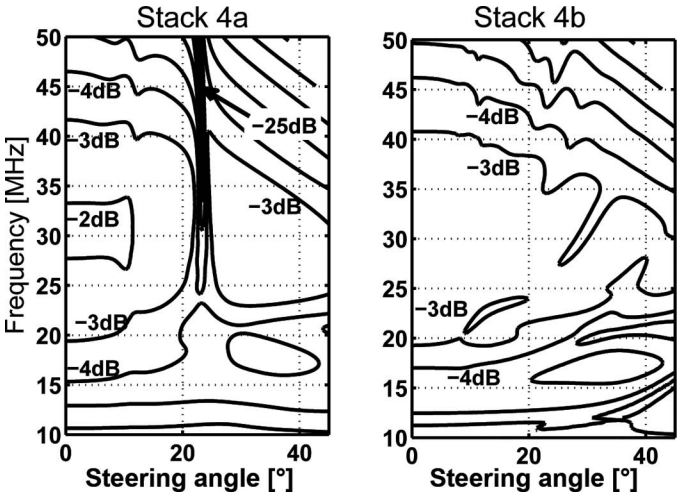

Fig. 10. Transmitted power as a function of frequency and steering angle from (left) Stack 4a and (right) Stack 4b. Stack 4b has a 100-μm intermediate damping layer between the CMUT array and the first circuit layer. The distance between contour lines is 1 dB.

that the pressure level variation along the array at high frequencies is severe. This might cause a dip in the amplitude of the transmitted pressure wave at this specific angle, which can give dark lines or spots in the image.

When focusing the same array at a distance equivalent of $300\lambda_c$, where λ_c is the wavelength at the center frequency, 30 MHz, we see from the upper pane of Fig. 12 that the maximum amplitude in the focal plane goes through a minimum around 17°. Higher frequencies lead to larger variations in the maximum amplitude. The lower pane of Fig. 12 shows how the side lobe level in the focal plane increases with frequency when the array is steered toward 17.75°. This is the steering angle at which the side lobe level is highest. Increased side lobe levels will cause image noise and poor focusing.

There is an interest in the ultrasound community to integrate PZT transducers with IC chips especially for high-frequency transducers [36]. We include an example in which we add a material on top of the CMUT array which has an acoustic impedance similar to a PZT composite. An impedance of 15 MRayl is chosen. The PZT impedance is then matched to the fluid. The stiffness and density of the CMUT membranes have been changed to give them approximately the same center frequency, bandwidth, and coupling coefficient as the CMUTs which operate in the fluid. The relation between the SAW and radiation into the fluid from this structure would be a crude model of how generation of SAW would affect the radiation from PZT-elements backed by a silicon chip.

The left plot of Fig. 13 shows that the dip in transmitted power for an infinite array with a 100-μm silicon substrate is deeper and wider when the acoustic impedance of the material directly above the silicon is higher. The variation of radiated pressure over the array surface of a finite array is considerably larger, as shown in the right plot of Fig. 13.

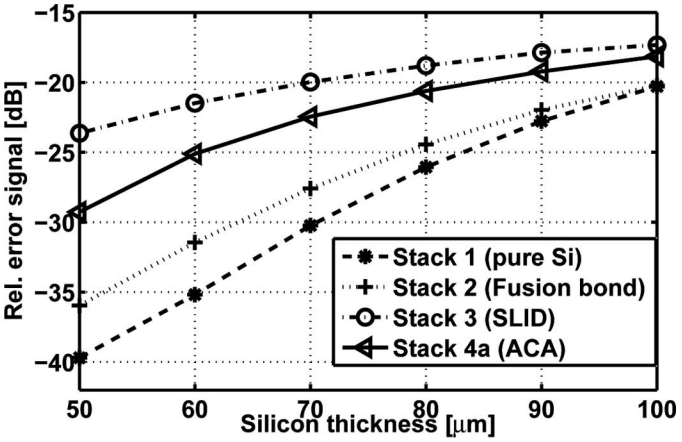

Fig. 9. Relative error signal integrated from 15 to 45 MHz, and over a 10° sector covering the steering angles for which the coupling to SAW is most severe.

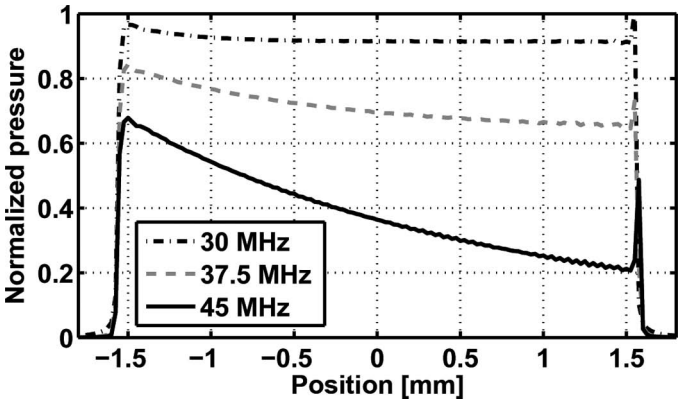

Fig. 11. Normalized radiated pressure from a 3.2-mm-wide array of CMUTs with a silicon substrate of 100 μm. Plan wave transmissions 17.75° off broadside at 30, 37.5, and 45 MHz are compared. The pressure is normalized to the maximum pressure from the array at 30 MHz with broadside transmission.

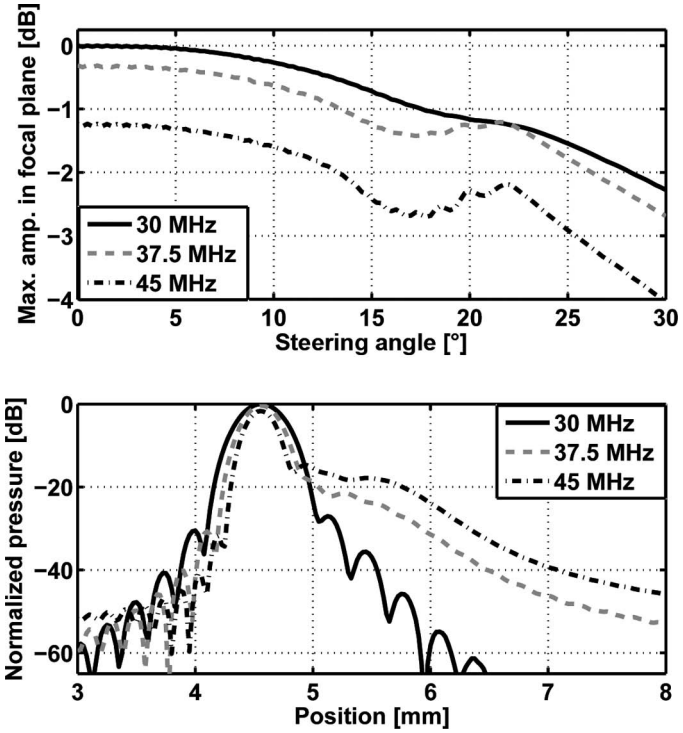

Fig. 12. (top) Maximum amplitude in the focal plane when focusing an array with a well-backed 100-μm silicon substrate at various angles at $300\lambda_c$ distance. (bottom) Comparison of the side lobe level in the focal plane at three different frequencies, when steering toward 17.75° off broadside. The pressure distributions for all frequencies are normalized to the maximum pressure at 30 MHz. A cosine squared weighting function has been applied to the excitation.

E. Reflection from the Bottom of the Acoustic Backing

An ideal backing material used in an ultrasound transducer would absorb all of the energy that is transmitted into it. However, if the transducer is to be mounted on an intravascular catheter there is limited space for the backing material. Because of this, there might be some reflectance back into the wafer stack. To minimize the specular backscattering with little space available, we may use a low-profile scattering structure at the bottom of the backing. This converts the incoming waves into waves with changed transverse k-vectors. Simulations indicate that an additional suppression of the specular reflection of approximately 10 dB can be achieved [37].

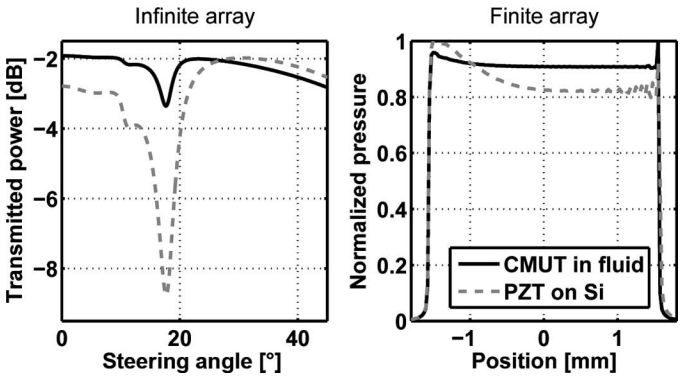

Fig. 13. Comparing the responses at 30 MHz from a CMUT array radiating into water and an array that mimics PZT mounted on top of silicon. (left) Transmitted power from infinite arrays. (right) Radiated normalized pressure from a 3.2-mm-wide array. In both cases, the silicon substrate is 100 μm thick, and it is backed with 200 μm of tungsten-epoxy backing.

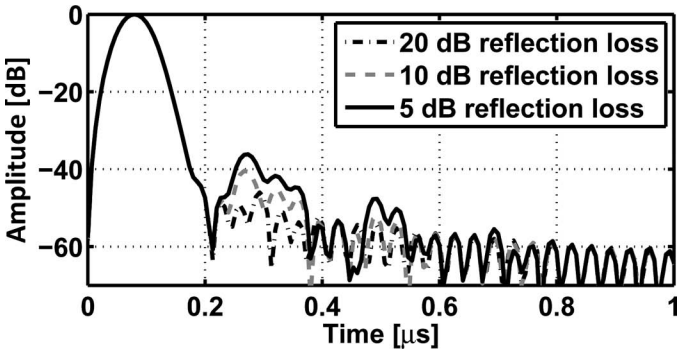

Fig. 14. Pulse response including the two-way impulse response of a CMUT array with 100-μm-thick silicon substrate, backed with 200-μm tungsten-epoxy. The response at 0° steering angle is shown for 5, 10, and 20 dB reduction of specular reflection at the array bottom. The array is excited by a cosine squared pulse covering the frequency range from 15 to 45 MHz.

In the calculations performed here, we only take into account the specular part of this reflection. In Figs. 6 through 13, the specular part is assumed to be reduced by 20 dB at the bottom of the acoustic backing material. In Fig. 14 we show that the ringing in the pulse response has higher amplitude if the reflection is reduced by only 5 or 10 dB instead of 20 dB.

V. Discussion

Array response degradation may be due to both excitation of SAW in the array structure, and excitation of bulk waves that travel deep into the array backing. The main interaction between the SAW in the substrate and the waves transmitted into rapeseed oil occurs between 15 and 30° steering angle. At certain steering angles, there is an increase in transmitted power into the fluid resulting from the SAW, because the SAW and the membranes are in phase. At other angles radiations are out of phase, and we get a minimum in the output signal. The angular position of the peak and dip in the power depends on the composition of the stack. Because the effect of the SAW is within the angular range commonly used in ultrasound imaging, it is important to consider this in the design process of CMUT arrays for imaging.

The three bonding techniques we have investigated have different advantages and drawbacks. The fusion bonding results in the best array response with regard to SAW effects. The process can be performed at room temperature and allows for high interconnect density. We base our simulations of fusion bonding on the DBI-technique presented by Ziptronix [24], where the bonding process results in an intermediate layer of SiO_2 of a few micrometers between the wafers. At the bond points, there are metal-to-metal

connections, but we assume that these are small in area and do not affect the acoustic response from the stack.

SLID bonding can be a good alternative. It has been shown feasible in MEMS 3-D stacking [23] and can provide high interconnect density. We have chosen a SLID bonding layer thickness of 8 μm, which corresponds to state-of-the-art as presented in the literature [23]. The SLID bonding layer consists of bottom and top layers of copper (Cu), which are 3 μm thick, and an intermediate 2-μm layer of Cu_3Sn. The fill factor of the metal layer must be accounted for. It must be high to obtain good acoustic contact between the wafers. In a real bonding situation, one probably must cover at least half of the area with metal. To achieve this, the alignment in the bonding process must be good. To ease calculations, we include the SLID layer on the entire area between the wafers. We find that the minimum SLID thickness found in literature is not satisfactory for applications at 30 MHz. Improvements of the technique are needed for it to be used in high-frequency ultrasound transducers.

In the simulations of the anisotropic adhesive, the physical contact between the metal particles and the metal contact pads is not assumed to influence the acoustic properties. Hence, the ACA is modeled as a uniform 2-μm layer of EPO-TEK 353. Available products of anisotropic films have particle sizes down to 2.5 μm, which will result in a bonding layer thickness of between 1 and 2 μm. ACA might be the easiest technique to use in a development phase because it does not require high temperature and sophisticated tools, but because of its acoustic properties, the substrate ringing is severe for 30-MHz transducers. Achieving thinner ACA layers calls for conductive particles in the sub-micrometer range and a high viscosity adhesive to get sufficiently thin glue layers.

When it comes to the composition and design of the acoustic backing material, there are many possible solutions. The scope of this work is not to give exact answers regarding the backing material, but to present simulation results showing that the specular reflection attenuation resulting from the backing should be in the range of 20 dB to avoid high-amplitude ringing in the pulse response. A low-profile scattering structure at the bottom of the backing might be of help if the space for backing material is limited. However, even though some energy is reflected from the backing, and reaches the top surface of the array, not all of it will be transmitted into the fluid outside the array. This is in part due to the high acoustic impedance of silicon compared with water, and also because the CMUT membranes are soft. Some of the energy will be transmitted, but much will be reflected or absorbed at the fluid-array interface.

The surface acoustic wave travels along the surface of the vibrating array. At the rim, it should be removed in some way, either absorbed or scattered into the damping material below the array. However, it might be challenging to find materials that completely remove the energy in the wave and, hence, some SAW may propagate back into the array.

In ultrasound imaging, the size of the transducer arrays vary depending on the application. Because the size of the array is an important factor determining how the generated surface acoustic wave will affect the image quality, one should be aware of this issue in transducer design. In large arrays, the SAW amplitude might become large, and the transmitted power from the array will hence decrease at angles where the excitation couples to the SAW. The simulations presented give some indications of possible effects on the image quality. How much distortion that can be accepted in an ultrasound image largely depends on the application.

The response curves given here, for an array at 30-MHz center frequency, apply for similar arrays at other frequencies, provided that all linear dimensions are scaled as the inverse of the center frequency, that all acoustic impedances are unchanged, and that the mechanical Q of the backing material is unchanged. Hence, arrays of lower center frequency might use thicker silicon substrates without experiencing problems with surface acoustic waves. Reducing the transmit frequency and increasing the element size will also make it possible to include more beamforming electronics on each circuit wafer. This might reduce the required number of wafers.

VI. Conclusion

To realize a 30-MHz intravascular ultrasound probe with CMUT array and integrated electronics we must use state of the art technologies for both circuit manufacturing and 3-D integration. The simulations presented show that making a 30 MHz CMUT array with a stack of three bonded integrated circuits is feasible if one allows a total silicon thickness below 100 μm. Fusion bonding shows the most promising results with regard to avoiding substrate ringing, whereas SLID and ACA bonding need some improvements when it comes to bonding layer thicknesses. However, they may be the easiest to implement.

The size of the transducer array affects how the surface acoustic wave develops, and whether its amplitude is high enough to distort the image quality at the angles at which the transmitted wave couples to the SAW. Hence, various applications may accept different levels of interactions with the surface acoustic wave before it affects the images in a severe manner.

If there is limited space for the backing material, one should take the possible reflections from the backing into account, and reflection reduction from the bottom of the backing should be implemented.

References

[1] I. Ladabaum, B. Khuri-Yakub, D. Spoliansky, and M. I. Haller, "Micromachined ultrasonic transducers (MUTs)," in *IEEE Ultrasonics Symp.*, 1995, pp. 501–504.

[2] I. Ladabaum, X. Jin, H. T. Soh, A. Atalar, and B. T. Khuri-Yakub, "Surface micromachined capacitive ultrasonic transducer," *IEEE*

Trans. Ultrason. Ferroelectr. Freq. Control, vol. 45, no. 3, pp. 678–690, May 1998.
[3] M. I. Haller and B. T. Khuri-Yakub, "A surface micromachined electrostatic ultrasonic air transducer," *IEEE Trans. Ultrason. Ferroelectr. Freq. Control*, vol. 43, no. 1, pp. 1–6, Jan. 1996.
[4] O. Oralkan, A. S. Ergun, J. A. Johnson, M. Karaman, U. Demirci, K. Kaviani, T. H. Lee, and B. T. Khuri-Yakub, "Capacitive micromachined ultrasonic transducers: Next-generation arrays for acoustic imaging?" *IEEE Trans. Ultrason. Ferroelectr. Freq. Control*, vol. 49, no. 11, pp. 1596–1610, 2002.
[5] C. H. Cheng, E. M. Chow, X. Jin, S. Ergun, and B. Khuri-Yakub, "An efficient electrical addressing method using through-wafer vias for two-dimensional ultrasonic arrays," in *IEEE Ultrasonics Symp.*, 2000, pp. 1179–1182.
[6] P.-C. Eccardt, K. Niederer, T. Scheiter, and C. Hierold, "Surface micromachined ultrasound transducers in CMOS technology," in *IEEE Ultrasonics Symp.*, 1996, pp. 959–962.
[7] R. A. Noble, R. R. Davies, M. M. Day, L. Koker, D. O. King, A. R. D. Jones, J. S. McIntosh, D. A. Hutchins, T. J. Robertson, and P. Saul, "A cost-effective and manufacturable route to the fabrication of high-density 2-D micromachined ultrasonic transducer arrays and (CMOS) signal conditioning electronics on the same silicon substrate," in *IEEE Ultrasonics Symp.*, 2001, pp. 941–945.
[8] R. A. Noble, R. R. Davies, D. O. King, M. M. Day, A. R. D. Jones, J. S. McIntosh, D. A. Hutchins, and P. Saul, "Low-temperature micromachined CMUTs with fully-integrated analogue front-end electronics," in *IEEE Ultrasonics Symp.*, 2002, pp. 1045–1050.
[9] C. Daft, S. Calmes, D. da Graca, K. Patel, P. Wagner, and I. Ladabaum, "Microfabrication ultrasonic transducers monolithically integrated with high voltage electronics," in *IEEE Ultrasonics Symp.*, 2004, pp. 493–496.
[10] C. Daft, P. Wagner, B. Bymaster, S. Panda, K. Patel, and I. Ladabaum, "cMUTs and electonics for 2D and 3D imaging: Monolithic integration, in-handle chip sets and system implications," in *IEEE Ultrasonics Symp.*, 2005, pp. 463–474.
[11] M. Hochmann, J. Zahorian, S. Satir, G. Furun, T. Xu, M. Karaman, P. Hasler, and F. L. Degertekin, "CMUT-on-CMOS for forward-looking IVUS: Improved fabrication and real-time imaging," in *IEEE Ultrasonics Symp.*, 2010.
[12] I. O. Wygant, X. Zhuang, D. T. Yeh, O. Oralkan, A. S. Ergun, M. Karaman, and B. T. Khuri-Yakub, "Integration of 2D CMUT array with front-end electronics for volumetric ultrasound imaging," *IEEE Trans. Ultrason. Ferroelectr. Freq. Control*, vol. 55, no. 2, pp. 327–342, 2008.
[13] P.-C. Eccardt, A. Lohfink, and H.-G. von Garssen, "Analysis of crosstalk between fluid coupled CMUT membranes," in *IEEE Ultrasonics Symp.*, 2005, pp. 593–596.
[14] X. Jin, Ö. Oralkan, F. L. Degertekin, and B. T. Khuri-Yakub, "Characterization of one-dimensional capacitive micromachined ultrasonic immersion transducer arrays," *IEEE Trans. Ultrason. Ferroelectr. Freq. Control*, vol. 48, no. 3, pp. 750–760, 2001.
[15] B. Bayram, M. Kupnik, G. G. Yaralioglu, Ö. Oralkan, D. Lin, X. Zhuang, A. S. Ergun, A. F. Sarioglu, S. H. Wong, and B. T. Khuri-Yakub, "Characterization of cross-coupling in capacitive micromachined ultrasonic transducers," in *IEEE Ultrasonics Symp.*, 2005, pp. 601–604.
[16] I. Ladabaum, P. Wagner, C. Zanelli, J. Mould, P. Reynolds, and G. Wojcik, "Silicon substrate ringing in microfabricated ultrasonic transducers," in *IEEE Ultrasonics Symp.*, 2000, pp. 943–946.
[17] X. Jin, F. L. Degertekin, S. Calmes, X. J. Zhang, I. Ladabaum, and B. T. Khuri-Yakub, "Micromachined capacitive transducer array for medical ultrasound imaging," in *IEEE Ultrasonics Symp.*, 1998, pp. 1877–1880.
[18] S. Berg and A. Rønnekleiv, "Backing requirements for CMUT arrays on silicon," in *IEEE Ultrasonics Symp.*, 2005, pp. 1952–1955.
[19] A. Rønnekleiv, "CMUT array modeling through free acoustic CMUT modes and analysis of the fluid CMUT interface through Fourier transform methods," *IEEE Trans. Ultrason. Ferroelectr. Freq. Control*, vol. 52, no. 12, pp. 2173–2184, 2005.
[20] S. Berg and A. Rønnekleiv, "Challenges with acoustic backing of CMUT arrays on silicon with integrated electronics," in *IEEE Ultrasonics Symp.*, 2009, pp. 980–983.
[21] P. Ramm, "Method of vertically integrating electric components by means of back contacting," U.S. Patent 6 548 391, Apr. 15, 2003.
[22] R. Wieland, D. Bonferst, A. Klumpp, R. Merkel, L. Nebrich, J. Weber, and P. Ramm, "3D integration of CMOS transistors with ICV-SLID technology," Microelectron. Eng., vol. 82, no. 3-4, pp. 529–533, 2005.
[23] M. M. Visser Taklo, M. M. Mielnik, K. Schjølberg-Henriksen, P. Storås, H. R. Tofteberg, N. Lietaer, and R. Johannesen, "Technologies enabling 3D stacking of MEMS," in *Smart System Integration and Reliability, Honorary Volume on Occasion of Herbert Reichl's 65th Birthday*, B. Michel and K.-D. Lang, Eds., Dresden, Germany: Goldenbogen-Verlag, 2010, pp. 136–145.
[24] Ziptronix Inc. (2012, Apr.) Direct bond interconnect. [Online]. Available: http://www.ziptronix.dreamhosters.com/technologies/dbi/.
[25] R. Chanchani, "3D integration technologies —An overview," in *Materials for Advanced Packaging*, New York, NY: Springer, 2009, ch. 1, pp. 1–50.
[26] P. J. Opdahl, (2012, Apr.) Anisotropic conductive film for flipchip applications: Introduction. [Online]. Available: http://flipchips.com/tutorial/assembly/anisotropic-conductive-film-for-flipchip-applications-introduction/
[27] R. S. Pai and K. K. Walsh, "The viability of anisotropic conductive film as a flip chip interconnect technology for MEMS devices," *J. Micromech. Microeng.*, vol. 15, no. 6, pp. 1131–1139, 2005.
[28] E. L. Adler, "Matrix methods applied to acoustic waves in multilayers," *IEEE Trans. Ultrason. Ferroelectr. Freq. Control*, vol. 37, no. 6, pp. 485–490, 1990.
[29] B. Bayram, E. Hæggström, G. G. Yaralioglu, and B. T. Khuri-Yakub, "A new regime for operating capacitive micromachined ultrasonic transducers," *IEEE Trans. Ultrason. Ferroelectr. Freq. Control*, vol. 50, no. 9, pp. 1184–1190, Sep. 2003.
[30] B. Auld, *Acoustic Fields and Waves in Solids*, vol. 1, 2nd ed., Malabar, FL: Krieger, 1990.
[31] D. Royer and E. Dieulesaint, *Elastic Waves in Solids I.* New York, NY: Springer, 2000.
[32] D. E. Gray, *American Institute of Physics Handbook*, 2nd ed., New York, NY: McGraw-Hill, 1963.
[33] X. Y. Pang, S. Q. Wang, L. Zhang, Z. Q. Liu, and J. K. Shang, "First principle calcuation of elastic and lattice constants of orthorombic Cu_3Sn crystal," *J. Alloy. Comp.*, vol. 466, no. 1–2, pp. 517–520, 2008.
[34] H. Wang, T. Ritter, W. Cao, and K. Shung, "High frequency properties of passive materials for ultrasonic transducers," *IEEE Trans. Ultrason. Ferroelectr. Freq. Control*, vol. 48, no. 1, pp. 78–84, 2001.
[35] A. J. Devaney and H. Levine, "Effective elastic parameters of random composites," *Appl. Phys. Lett.*, vol. 37, no. 4, pp. 377–379, Aug. 1980.
[36] W. Ossmann, B. J. Savord, J. Chen, and R. J. Solomon, "Integrated circuit with spurrious acoustic mode suppression and method of manufacture thereof," U.S. Patent Application, pub. no. 2011/0254109 A1, Oct. 20, 2011.
[37] K. Chapagain and A. Rønnekleiv, "Minimizing the bottom reflections in ultrasonic CMUT transducer backing using low profile structuring," in *IEEE Ultrasonics Symp.*, 2009, pp. 430–433.

Sigrid Berg was born in Tromsø, Norway, in 1978. She received her B.Sc. and M.Sc. degrees from the Department of Engineering Cybernetics at the Norwegian University of Science and Technology (NTNU), Trondheim, Norway, in 2002 and 2004, respectively. She is currently working on her Ph.D. degree in the Electronic Devices and Materials group at the Department of Electronics and Telecommunications at the same university. Her Ph.D. work mainly involves simulations and measurements of crosstalk in capacitive micromachined ultrasonic transducers (CMUTs).

Arne Rønnekleiv (M'94) was born in Telemark, Norway, on February 14, 1941. He earned his Siv.Ing. degree in 1966, and his Lic.Techn. degree in 1970 at NTH. Since 1971, he has been employed at NTH, later renamed the Norwegian University of Science and Technology (NTNU), in the Division of Electronics and Telecommunications, since 1986 as professor. He is now professor emeritus. He has directed much of his scientific and technical work toward the design and application of components based on SAWs, and in the later years, CMUTs for medical applications. He is an IEEE member.